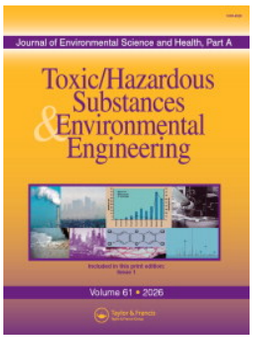

Taylor & Francis
Taylor & Francis Group

Journal of Environmental Science and Health, Part A
Toxic/Hazardous Substances and Environmental Engineering

ISSN: 1093-4529 (Print) 1532-4117 (Online) Journal homepage: www.tandfonline.com/journals/lesa20

Development of KOH-impregnated activated carbon from coal for carbon dioxide capture

Deepesh Kumar Biswal , Dipa Das, Kashinath Barik & Sushanta Kumar Behera

To cite this article: Deepesh Kumar Biswal , Dipa Das, Kashinath Barik & Sushanta Kumar Behera (05 Mar 2026): Development of KOH-impregnated activated carbon from coal for carbon dioxide capture, Journal of Environmental Science and Health, Part A, DOI: 10.1080/10934529.2026.2636414

To link to this article: https://doi.org/10.1080/10934529.2026.2636414

Published online: 05 Mar 2026.

JOURNAL OF ENVIRONMENTAL SCIENCE AND HEALTH, PART A
https://doi.org/10.1080/10934529.2026.2636414

Development of KOH-impregnated activated carbon from coal for carbon dioxide capture

Deepesh Kumar Biswal[a,b], Dipa Das[a], Kashinath Barik[a], and Sushanta Kumar Behera[c]

[a]Department of Chemical Engineering, Indira Gandhi Institute of Technology (IGIT), Sarang, Odisha, India; [b]State Pollution Control Board (SPCB), Koraput, Odisha, India; [c]Department of Chemical Engineering, National Institute of Technology (NIT) Andhra Pradesh, Tadepalligudem, India

ABSTRACT

With increasing globalization and industrialization, reducing carbon dioxide (CO_2) emissions has become a critical global challenge. The objective of this study was to investigate the potential of coal-derived activated carbon (AC) for CO_2 adsorption under environmentally relevant conditions. In the present study, AC derived from peat and lignite coal was synthesized by a chemical activation method using a wide range of KOH with impregnation ratios (1:1, 1:2, 1:4, 1:6, and 1:8), enabling precise control over micropore development. This study identifies the optimum impregnation ratio that maximizes the ultra-micropore volume, which is directly responsible for enhanced CO_2 adsorption. The prepared materials were systematically characterized by proximate and ultimate analyses, Brunauer–Emmett–Teller surface area measurements, thermogravimetric analysis, Fourier-transform infrared spectroscopy, X-ray diffraction, and scanning electron microscopy. CO_2 adsorption experiments were conducted by the Autosorb iQ gas sorption analyzer at near-ambient temperature and pressure. The lignite-derived AC at a 1:8 impregnation ratio showed the highest CO_2 uptake (46.27 mg g^{-1}) with a breakthrough time of 204.7 min. The most important novelty of our work is the productive utilization of low-grade coal, as a viable precursor and aim is to convert such low-grade coal for the production of high-performance and cost-effective CO_2 adsorbents, which aligns with sustainable materials development and carbon management.

ARTICLE HISTORY
Received 27 November 2025
Accepted 19 February 2026

KEYWORDS
Activated carbon; adsorption; carbon dioxide; impregnation ratio; coal; peat; lignite

Introduction

The rapid expansion of industrialization, coupled with the intensification of the greenhouse effect, has emerged as a critical global concern. The greenhouse effect is mainly caused by the release of greenhouse gases (GHGs). The most significant of these is carbon dioxide (CO_2), followed by nitrous oxide (N_2O), sulfur hexafluoride (SF_6), chlorofluorocarbons, and methane (CH_4). This situation has put the Earth's ecological balance in serious danger since industrial development began. In the last hundred years, the world's average temperature has risen by about 0.74 °C. Predictions suggest that it could increase by as much as 6.4 °C by the end of this century, which is a serious threat to both the environment and our social and economic stability.[1] Carbon dioxide (CO_2) is the most important GHG produced by human activities, attracting considerable attention from scientists and policymakers. It is crucial to track and reduce CO_2 emissions to lessen the negative effects that climate change brings.[2] Increasing CO_2 levels, along with other GHGs, are the main causes of global warming, leading to severe issues like droughts, floods, heat waves, and harm to ecosystems. The economic impact of climate change is significant, with estimates suggesting 5–20% of the world's GDP.[3] Furthermore, long-term effects include erosion of coastlines, changes in farming seasons, melting glaciers, and rising sea levels. The situation is worsened by extreme weather events such as typhoons, cyclones, floods, and droughts, along with the depletion of the ozone layer.[4–5] The combustion of fossil fuels like natural gas, coal, and oil produces over 95% of yearly CO_2 emissions, while the rest comes from industrial processes like generating electricity, making cement, and producing steel, iron, and ammonia.[6–10] Although natural events like forest fires, volcanic eruptions, and the breakdown of organic matter do add to emissions, their levels tend to stay steady over time.[11] To tackle these issues, it is essential to lower GHG emissions. Carbon capture and storage (CCS) technologies are seen as crucial for reducing human-made emissions and promoting climate stability.[12–15] For CCS to work effectively, it needs to be both energy-efficient and cost-effective. Common carbon capture methods encompass pre-combustion, post-combustion, oxy-fuel combustion, and chemical looping combustion techniques.[16] The subsequent CO_2 separation stage is typically achieved by one of four approaches: absorption, cryogenic distillation, membrane separation, or adsorption. Among these, adsorption is considered the most promising due to

CONTACT Dipa Das dipa.das80@gmail.com, dipadas@igitsarang.ac.in Department of Chemical Engineering, Indira Gandhi Institute of Technology (IGIT), Sarang, Odisha 759146, India

its low energy requirements, simple process design, and non-corrosive nature.[17] Both physisorption and chemisorption are widely studied, with current research emphasizing the development of sorbents possessing optimal structural and chemical characteristics for efficient CO_2 capture. Well-established sorbents include activated carbon (AC), zeolites, metal-organic frameworks, graphene, and alkali- or alkaline earth-based sorbents (e.g. potassium-, lithium-, and calcium-based materials). Of these, AC stands out as the most versatile due to its high adsorption capacity, large surface area, and tunable pore structure. ACs are typically derived from carbonaceous materials with high carbon content, low ash content, and significant volatile matter, prepared through physical activation, chemical activation, or a combination of both. Structurally, ACs are highly porous and heterogeneous, with cylindrical, rectangular, or irregular pores spanning across micropores (<2 nm), mesopores (2–50 nm), and macropores (>50 nm).[18] AC generally exhibits a high surface area in the range of 700–1800 m^2 g^{-1},[19] along with favorable properties such as high thermal stability, low acid–base reactivity, adjustable surface chemistry, hydrophobicity, stability under ambient conditions, and ease of regeneration.[20] Its adsorption performance is strongly influenced by surface functional groups, precursor type, and the activation technique employed, all of which govern the pore distribution and surface area. Importantly, the impregnation ratio of the activating agent serves as a key parameter in tuning surface properties, enhancing both the surface area and pore volume of the material. Based on the literature, biomass-derived and chemically ACs highlight the importance of optimized activation strategies and micropore development for enhanced CO_2 adsorption. KOH-ACs derived from Borassus flabellifer flower reported by Tonu et al. exhibit the maximum CO_2 adsorption capacities, 4.8 mmol g^{-1} due to increased microporosity.[21] Kundu et al. discussed the tradeoff between high impregnation ratios, adsorption performance, process economics, and pore structure tuning critically influence CO_2 adsorption behavior in biomass-derived carbons.[22] Deng et al. further demonstrated that controlled activation condition can yield competitive CO_2 adsorption with improved sustainability and cyclic stability of biochar.[23] Khandaker et al. emphasize the growing interest in low-cost carbonaceous feedstocks for CO_2 capture applications.[24] Wang et al. studied on one-step KOH activation of lignite coal leading to CO_2 capture of 1.35 mmol g^{-1} after optimization of impregnation ratio and activation conditions.[25] Labus et al. studied KOH activation of coal-produced microporous AC with high CO_2 uptake, 6.2 mmol g^{-1} at 273 K.[26] Chemical impregnation significantly alters the textural properties of AC, including pore structure and surface area, thereby affecting its adsorption capacity and overall performance. Careful optimization of the impregnation ratio is indispensable for customizing AC for specific end uses, while simultaneously considering porosity development, material yield, and cost-effectiveness. Gaining deeper insight into the relationship between impregnation ratio and carbon characteristics is fundamental for refining fabrication processes and producing ACs with enhanced functional performance.[22]

Although the KOH-activated coal-derived AC has been previously reported for CO_2 adsorption, the most important novelty of our work is the productive utilization of low-grade coal, which is often underutilized or environmentally problematic. So, our aim is to convert such coal into high-performance CO_2 adsorbents, which aligns with sustainable materials development and carbon management strategies. In this context, the present study investigates the synthesis and characterization of coal-derived AC derived from peat and lignite coal, chemically activated using KOH at varying impregnation ratios. A wide range of KOH impregnation ratios, enabling precise control over micropore development. This study identifies the optimum impregnation ratio that maximizes the ultramicropore volume, which is directly responsible for enhanced CO_2 adsorption. which is more relevant for practical post-combustion CO_2 capture, demonstrating its applicability beyond laboratory-scale evaluations. with the objective of optimizing CO_2 adsorption performance. The outcomes provide insights into the development of cost-effective and sustainable adsorbents for carbon capture applications. In light of these studies, the present work demonstrates that lignite-derived AC prepared at an optimized impregnation ratio (1:8) achieves a CO_2 adsorption capacity of 46.27 mg g^{-1} at near-ambient temperature and pressure with excellent thermal stability, offering a cost-effective and scalable alternative to biomass-derived carbons.

Materials and experimental procedure

Materials

Peat and lignite coal samples were procured from Bharatpur OCP, Talcher, and used as precursors for the synthesis of AC. Analytical-grade potassium hydroxide (KOH), hydrochloric acid (HCl, 0.5 N), and distilled water were employed in the activation and washing processes. High-purity nitrogen gas (>99.99%) was used as the inert atmosphere during carbonization.

Preparation of AC from coal

The collected coal samples were initially washed with running water to remove surface impurities and subsequently sun-dried. Further drying was carried out in a hot-air oven at 100 °C until constant weight was achieved. The dried samples were crushed using a mortar and pestle, followed by sieve analysis to obtain particle size fractions in the range of 500–250 µm. For AC synthesis, particles within the 250–300 µm range were selected. For chemical activation, KOH was used as the activating agent because during high-temperature activation, KOH promotes carbon etching through redox reactions and intercalation mechanisms, leading to the formation of narrow micropores that are particularly favorable for CO_2 adsorption *via* pore-filling interactions. 1 M KOH solution was prepared by dissolving 56 g of KOH pellets in 1000 mL of distilled water. Approximately 50 g of

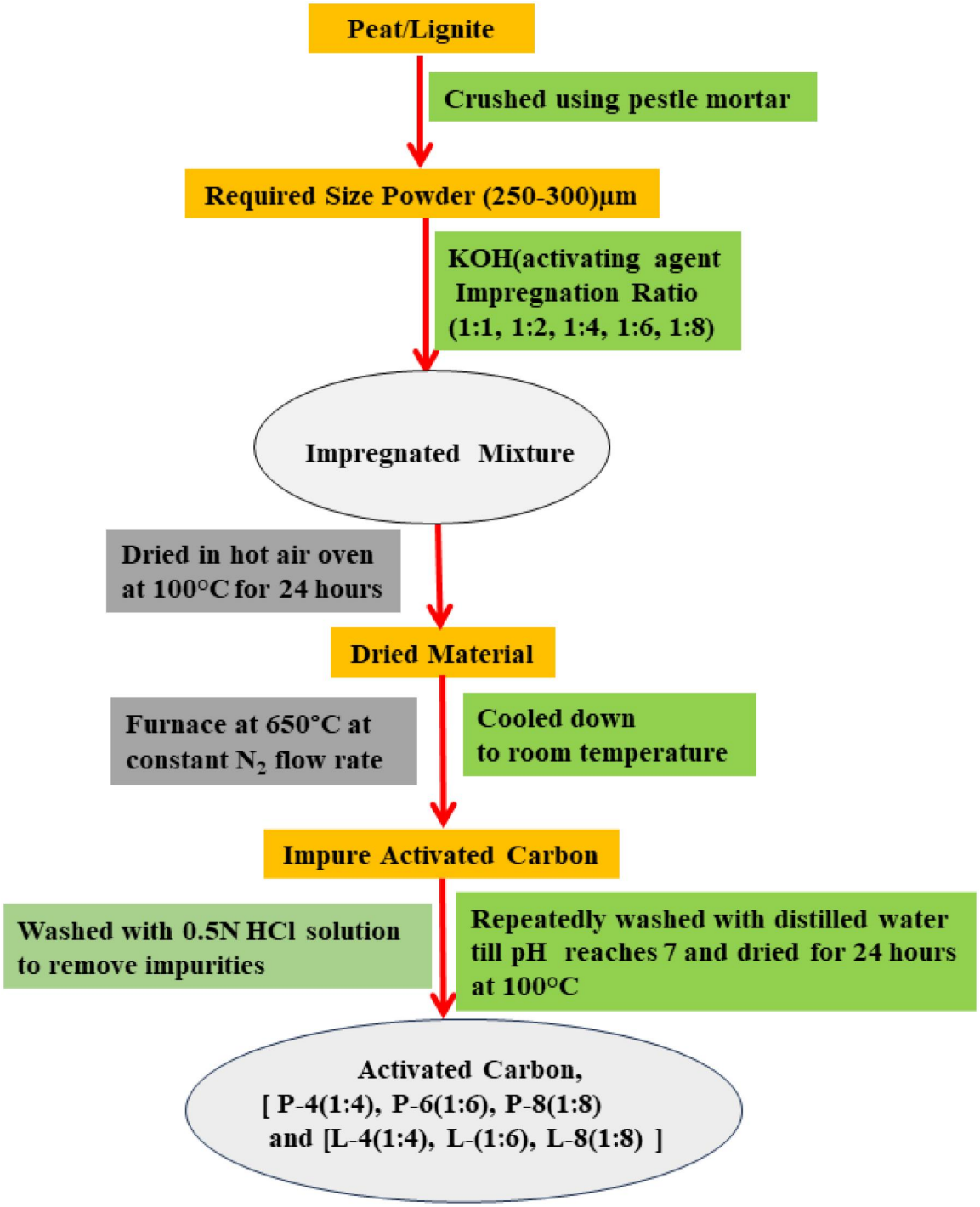

Figure 1. Flow diagram for the preparation of activated carbon.

each coal sample (peat and lignite) was impregnated with KOH solution at different impregnation ratios (1:1, 1:2, 1:4, 1:6, and 1:8). The resulting slurry was kept for 24 h to ensure uniform impregnation. Following impregnation, the samples were oven-dried at 100 °C for 24 h, cooled, and stored in a desiccator. The dried samples were then placed inside galvanized iron pipes (inner diameter 4.95 cm, outer diameter 5 cm, length 20 cm) and subjected to carbonization in a muffle furnace under a continuous flow of nitrogen (120 cm^3 min^{-1}, STP). Carbonization was carried out at four different temperatures (550 °C, 650 °C, 750 °C, and 850 °C), each for a duration of 1 h. After heat treatment, the furnace was allowed to cool under constant nitrogen flow until the samples reached room temperature. The carbonized samples were washed repeatedly (2–3 times) with 0.5 N HCl to remove residual inorganic matter, followed by warm distilled water, and finally rinsed with cold distilled water until the wash solution reached neutral pH (confirmed using pH paper). The samples were then oven-dried at 100 °C for 24 h and stored in airtight zipper bags.[27–31]

The prepared samples were labeled according to coal type and impregnation ratio, e.g. P-1 (peat, 1:1), L-1 (lignite, 1:1), and so forth. The overall preparation process flow diagram for AC is illustrated in Figure 1.

Table 1. Proximate analysis of activated carbons from peat.

Sample	Moisture content (%)	Volatile matter (%)	Ash content (%)	Fixed carbon (%)
Raw peat	9	40.85	4.21	45.94
P-1(1:1)	7.15	24.97	0.73	67.15
P-2(1:2)	6.98	24.35	0.82	67.85
P-4(1:4)	6.54	23.84	0.93	68.69
P-6(1:6)	4.78	23.04	2.11	70.07
P-8(1:8)	4.19	21.35	2.98	71.48

Table 2. Proximate analysis of activated carbon from lignite.

Sample	Moisture content (%)	Volatile matter (%)	Ash content (%)	Fixed carbon (%)
Raw lignite	8	41.27	3.51	47.22
L-1(1:1)	6.11	24.98	0.65	68.26
L-2(1:2)	5.98	24.87	0.73	68.42
L-4(1:4)	4.79	24.45	0.78	69.98
L-6(1:6)	3.68	24.64	0.95	70.73
L-8(1:8)	3.21	23. 89	1.45	72.45

Characterization of coal-based AC

Proximate analysis was performed to determine the moisture content, volatile matter, fixed carbon, and ash content of the raw precursors and synthesized AC samples. Ultimate analysis was performed using a Vario MACRO cube elemental analyzer to evaluate the elemental composition of the adsorbents. Surface properties were analyzed using a Micromeritics 3Flex analyzer. N_2 adsorption–desorption at 77 K was used to determine Brunauer–Emmett–Teller (BET) surface area and pore characteristics. The morphology of the samples was analyzed by FE-SEM (JSM-7610F, JEOL, Japan). Surface functionalities were identified by Fourier-transform infrared (FTIR) spectroscopy using PerkinElmer Frontier. Thermogravimetric analysis (TGA) was performed using a PerkinElmer TGA 4000 under a nitrogen atmosphere at a constant heating rate. to study the thermal stability and weight loss profile of the adsorbents with respect to temperature and time. Crystalline structure was investigated by X-ray diffraction (XRD) using a PANalytical X'Pert PRO diffractometer (Malvern PANalytical, The Netherlands) with Cu Kα radiation. CO_2 adsorption measurements were further conducted using gas sorption analyzer(Autosorb iQ and ASiQwin) manufactured by Quanta Chrome Instrument, USA (Version 3.0)

CO_2 capture experimental procedure

Batch adsorption experiments were conducted using an Autosorb iQ analyzer by the static volumetric method. Equilibrium adsorption was determined by pressure stabilization. Three consecutive adsorption–desorption cycles were carried out, with complete evacuation between cycles, to evaluate reversibility and adsorption stability. The CO_2 uptake was calculated automatically by the instrument software to generate adsorption isotherms. All adsorption experiments were conducted under well-controlled and stable conditions. Prior to measurements, samples were degassed under vacuum, and adsorption isotherms were collected over a wide pressure range.

Results and discussion

Proximate analysis

Proximate analysis was conducted to evaluate the moisture, volatile matter, fixed carbon, and ash content of the raw precursors (peat and lignite coal) and the AC samples prepared at different impregnation ratios. The results for peat- and lignite-derived AC are summarized in Tables 1 and 2. For peat, the fixed carbon content in the raw precursor was 45.94%. Among the prepared ACs, the sample with an impregnation ratio of 1:8 (P-8) exhibited the highest fixed carbon content (71.48%). In the case of lignite coal, the initial precursor was found to have 47.22% fixed carbon. Meanwhile, the AC produced from lignite, which had an impregnation ratio of 1:8 (L-8), displayed a peak fixed carbon content of 72.45%. As the impregnation ratio increased, both precursors showed an improvement in fixed carbon content along with a decrease in volatile matter. This phenomenon can be explained by the stronger reaction that occurs between the carbon matrix and the activating agent (KOH), prompting the release of gaseous byproducts like CO_2 and CO. Such reactions play a vital role in creating micropores on the surface of the carbon, thus boosting the fixed carbon content. Additionally, a rise in the activation temperature led to an increase in fixed carbon content while simultaneously decreasing the volatile matter in the coal samples.[32,33] The ash content in the ACs produced from both peat and lignite materials was observed to be quite low, which is beneficial for adsorption purposes.

Ultimate analysis

An ultimate analysis of adsorbents was conducted to find out the elemental percentage of carbon, hydrogen, nitrogen, sulfur, and oxygen for both the raw materials and AC samples as shown in Tables 3 and 4. For the raw materials, the carbon percentages were 41.65% for peat and 42.71% for lignite. After activation, a notable increase in carbon content was detected. The AC created with an impregnation ratio of 1:8 displayed the highest levels of carbon, reaching 65.64% for P-8 and 70.57% for L-8, respectively. The rise in carbon

Table 3. Ultimate analysis of AC from peat.

Sample	Nitrogen (%)	Carbon (%)	Hydrogen (%)	Sulfur (%)	Oxygen (%)
Raw peat	0.82	41.65	8.91	18.95	28.67
P(1:1)	6.14	58.15	3.08	0.44	32.19
P(1:2)	6.09	59.98	3.95	0.72	29.26
P(1:4)	5.97	61.78	4.12	0.95	27.18
P(1:6)	5.37	62.15	5.35	1.08	26.05
P(1:8)	3.94	65.64	3.05	1.38	25.99

Table 4. Ultimate analysis of AC from lignite.

Sample	Nitrogen (%)	Carbon (%)	Hydrogen (%)	Sulfur (%)	Oxygen (%)
Raw	3.16	42.71	9.34	31.87	12.92
L(1:1)	6.89	66.50	2.95	0.17	23.49
L(1:2)	6.54	67.83	3.05	0.19	22.39
L(1:4)	5.97	68.78	3.12	0.25	21.88
L(1:6)	4.87	69.15	3.35	0.98	21.65
L(1:8)	7.03	70.57	2.49	0.34	19.57

levels with increased impregnation ratios is due to the loss of volatile substances and the formation of a porous structure during the activation process. When examining the sulfur content in all the samples, it was noted that it is relatively low compared to other elements.[32–33] This is beneficial for adsorption purposes, as it reduces the chance of harmful sulfur compounds being released during use. These results indicate that ACs treated with KOH have favorable elemental properties, which make them effective options for CO_2 adsorption.

Brunauer–Emmett–Teller analysis

The BET analysis serves as a dependable technique for assessing the surface characteristics of porous solids, which includes examining their specific surface area, pore volume, and distribution of pore sizes. Typically, a larger surface area indicates higher reactivity and better adsorption capacity. The adsorption isotherms obtained were evaluated using the BET equation to determine the surface area, while the pore size distribution was achieved through the Barrett–Joyner–Halenda (BJH) method and density functional theory. The microporous surface area (S_{micro}) and the micropore volume (V_{micro}) were identified using the *t*-plot technique. Tables 5 and 6 provide a summary of the textural characteristics of ACs made from peat and lignite, highlighting variations based on different impregnation ratios and activation temperatures.

Raw peat and lignite samples exhibited relatively low BET surface areas, micropore areas, and micropore volumes. Upon KOH activation at impregnation ratios of 1:1 to 1:8 and carbonization temperatures of 550–850 °C, a substantial improvement in these parameters was observed. Peat-derived AC with an impregnation ratio of 1:8 (P-8) exhibited progressive increases in BET surface area 766.25–799.48 $m^2\ g^{-1}$, micropore area 737.38–776.64 $m^2\ g^{-1}$, and micropore volume 0.394–0.431 $cm^3\ g^{-1}$ as the carbonization temperature increased from 550 °C to 850 °C. Similarly, lignite-derived AC at the same ratio (L-8) showed BET surface area values rising from 818.64 to 902.46 $m^2\ g^{-1}$, micropore area from 764.86 to 853.29 $m^2\ g^{-1}$, and micropore volume from 0.175 to 0.190 $cm^3\ g^{-1}$ across the same temperature range.[34] It was further observed that beyond certain activation conditions, excessive carbonization could cause pore collapse or merging, leading to a decline in surface area. However, within the studied range, both impregnation ratio and activation temperature had a positive effect on the development of surface area and pore volume. Among all the samples, L-4(1:4), L-6(1:6), and particularly L-8(1:8) exhibited the highest surface area and micropore volume which are desirable for adsorption applications due to strong interactions between micropores and adsorbates. Chemically activated with KOH improves the specific surface area of the carbon materials. Impregnation of more KOH results in a progressive increase in surface area and total pore volume due to chemical reactions between KOH and the carbon framework, resulting in the formation of potassium carbonate and then it decomposes at elevated temperatures. The generation and breakdown of K_2CO_3 above 500 °C creates micropores within the carbon matrix, resulting in enhanced textural properties. The reaction between KOH and CO_2 plays an important role in pore development with the formation of potassium carbonate as shown in Eq. (1):

$$2KOH + CO_2 \rightarrow K_2CO_3 + H_2O \quad (1)$$

In the subsequent step, the potassium carbonate decomposes near 600 °C, contributing to pore formation of micropore inside the carbon matrix, leading to an increase in specific surface area and total pore volume.[35]

Nitrogen adsorption–desorption isotherms and pore size distribution

Figures 2–4 present the nitrogen adsorption isotherms of L-4(1:4), L-6(1:6), and L-8(1:8) AC samples treated at 923.15 K for 1 h, within the relative pressure (P/P_0) range of 0.01–0.99. An isotherm is a graphical representation that depicts adsorption behavior at a constant temperature. In this case, the adsorption isotherms were obtained at standard conditions ($T = 77$ K, $p = 1$ atm) by plotting the volume of N_2 adsorbed versus relative pressure. The isotherms indicate that with increasing relative pressure, the volume of nitrogen adsorbed also increases, suggesting the presence of abundant micropores in the AC samples. The maximum N_2 adsorption capacities of L-4(1:4), L-6(1:6), and L-8(1:8) were 297.27, 281.69, and 247.14 cc g^{-1}, respectively. Based on the International Union of Pure and Applied Chemistry (IUPAC) classification, all three samples exhibit Type I isotherms, which are characteristic of microporous structures with strong adsorbate–adsorbent interactions.[36] At very low relative pressures ($P/P_0 \approx 0.0$), significant adsorption occurs due to the filling of micropores. The adsorption capacities at this stage were highest for the L-4(1:4) sample (220 cc g^{-1}), followed by L-6(1:6) (205 cc g^{-1}), and lowest for L-8(1:8) (140 cc g^{-1}). This trend indicates that although L-8(1:8) has a high BET surface area and total pore volume, the initial micropore filling is more pronounced in L-4(1:4) and L-6(1:6).

Furthermore, the pore size distribution determined by the BJH method is shown in Figures 5–7 for the three samples. The BJH analysis confirms the predominance of micropores (<2 nm) with narrow pore size distributions, validating the

Table 5. BET analysis of AC from peat.

Sample name	Temperature (°C)	S_{BET} (m^2 g^{-1})	Micropore area (m^2 g^{-1})	Micropore volume (cm^3 g^{-1})	Total pore volume (cm^3 g^{-1})
P-1(1:1)	550	594.67	566.37	0.210	0.297
	650	598.32	571.22	0.221	0.326
	750	605.79	580.53	0.246	0.343
	850	611.12	589.34	0.268	0.365
P-2(1:2)	550	618.36	592.11	0.289	0.386
	650	621.35	601.27	0.290	0.387
	750	632.78	612.54	0.299	0.396
	850	639.24	619.76	0.311	0.408
P-4(1:4)	550	669.31	642.41	0.324	0.421
	650	678.54	655.88	0.347	0.444
	750	689.67	661.52	0.361	0.458
	850	700.52	673.85	0.372	0.469
P-6(1:6)	550	717.58	692.41	0.379	0.476
	650	729.22	701.01	0.384	0.481
	750	741.51	706.46	0.387	0.484
	850	752.98	714.86	0.390	0.487
P-8(1:8)	550	766.25	737.38	0.394	0.491
	650	781.22	749.11	0.397	0.494
	750	792.35	768.23	0.418	0.515
	850	799.48	776.64	0.431	0.528

Table 6. BET analysis of AC from lignite.

Sample name	Temperature (°C)	S_{BET} (m^2 g^{-1})	Micropore area (m^2 g^{-1})	Micropore volume (cm^3 g^{-1})	Total pore volume (cm^3 g^{-1})
L-1(1:1)	550	619.92	606.24	0.09	0.149
	650	624.58	611.52	0.101	0.160
	750	631.24	618.59	0.104	0.163
	850	646.66	621.13	0.108	0.167
L-2(1:2)	550	653.14	624.23	0.110	0.169
	650	657.35	625.78	0.111	0.170
	750	663.49	637.28	0.112	0.171
	850	678.14	651.37	0.114	0.173
L-4(1:4)	550	693.55	671.89	0.116	0.175
	650	712.54	688.23	0.120	0.179
	750	728.86	697.34	0.131	0.190
	850	749.21	719.24	0.138	0.197
L-6(1:6)	550	767.33	727.16	0.149	0.208
	650	782.31	739.57	0.156	0.215
	750	793.12	745.65	0.160	0.219
	850	802.14	756.44	0.169	0.228
L-8(1:8)	550	818.64	764.86	0.175	0.234
	650	827.28	778.11	0.179	0.238
	750	842.37	789.62	0.187	0.246
	850	902.46	853.29	0.190	0.249

microporous nature of the synthesized ACs. The present study is limited by the number of repeat measurements, and therefore, the conclusions are based on comparative trends.

TGA

The weight–temperature curves of the AC samples L-4(1:4), L-6(1:6), and L-8(1:8), shown in Figures 8–10, reveal distinct weight loss behaviors, highlighting the changes in mass with increasing temperature. TGA of the samples can be divided into three main stages. At the initial stage, i.e. at 150 °C, a small mass loss occurs due to the evaporation of surface and bound water, as well as the release of light volatile organic compounds and impurities. Thermal decomposition occurs within the temperature range 150–500 °C. A gradual weight loss is observed as the organic structure decomposes. Volatile components such as hydrocarbons and CO_2 are released. This stage involves both endothermic and exothermic processes, depending on the chemical nature of the sample. Residual stabilization occurs when the temperature is more than 500 °C. At higher temperatures, stabilization of the residual material occurs, which primarily consists of nonvolatile inorganic components such as ash and metal oxides. In the presence of oxygen, oxidation of the fixed carbon may also take place. This stage is often marked by a sharp decline in mass (steep slope), indicating severe degradation or erosion of the material.

As the temperature increased from room temperature to 800 °C, the total weight loss observed for L-4(1:4), L-6(1:6), and L-8(1:8) were 12.44%, 10.67% and 9.42% respectively. The results clearly demonstrate that L-8(1:8) exhibits the lowest weight loss, confirming its superior thermal stability compared to L-4(1:4) and L-6(1:6). This enhanced stability is attributed to effective KOH impregnation, which improves the structural resistance of AC against thermal degradation and surface erosion. Consequently, L-8(1:8) emerges as the most thermally stable sample, making it highly suitable for industrial applications where thermal resistance is critical.

FTIR spectroscopy

FTIR spectroscopy provides valuable insight into the functional groups present on the surface of AC samples. When a

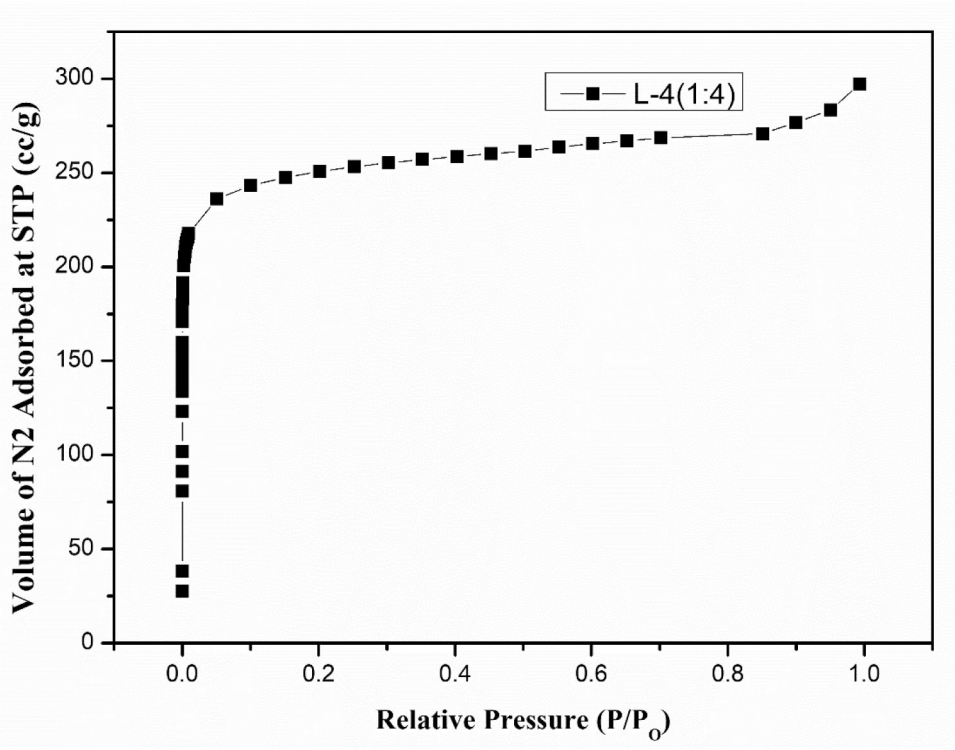

Figure 2. Volume of nitrogen adsorbed for L-4(1:4).

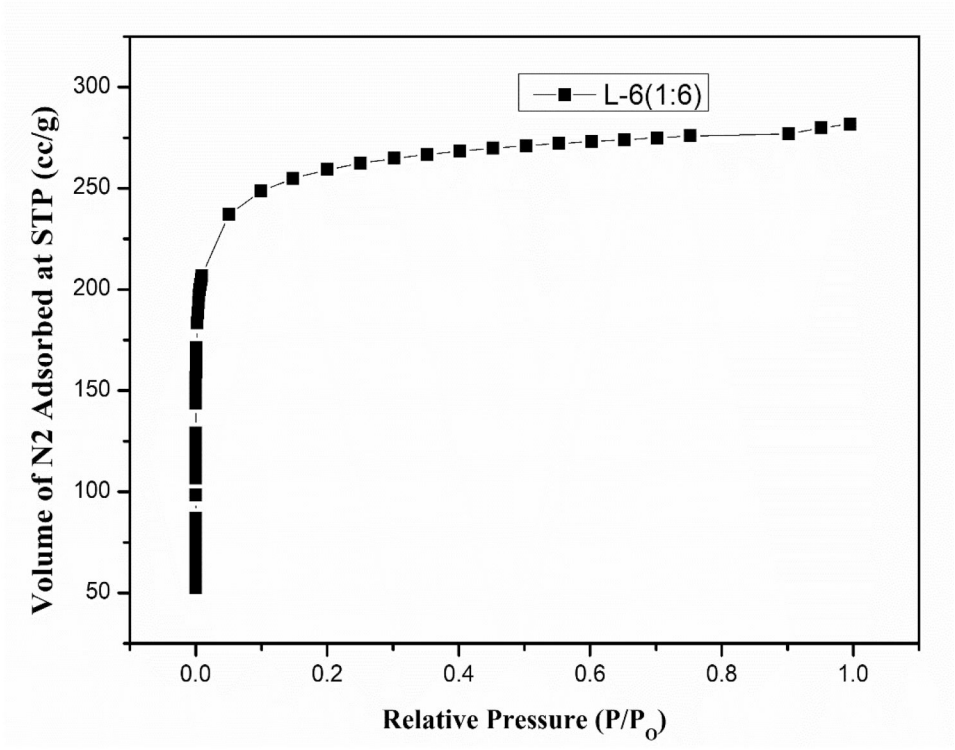

Figure 3. Volume of nitrogen adsorbed for L-6(1:6).

material is exposed to infrared radiation, molecular vibrations occur, leading to absorption or transmission at specific frequencies determined by the chemical bonds and structure of the sample. The resulting interferogram is mathematically converted into an infrared spectrum using the Fourier transform. The FTIR spectra of samples L-4(1:4), L-6(1:6), and L-8(1:8) are shown in Figures 11–13. The presence of functional groups such as carboxyl, amines, nitro, hydroxyl, and alcohol groups plays a crucial role in determining the CO_2 adsorption capacity of the materials. L-4(1:4) and L-6(1:6) display strong C–H bending vibrations corresponding to 1,2,4-trisubstituted aromatic rings, whereas these features are absent in L-8(1:8). Instead, L-8(1:8) exhibits a medium C = C bending peak at 836.99 cm^{-1}, confirming the presence of alkenes. This

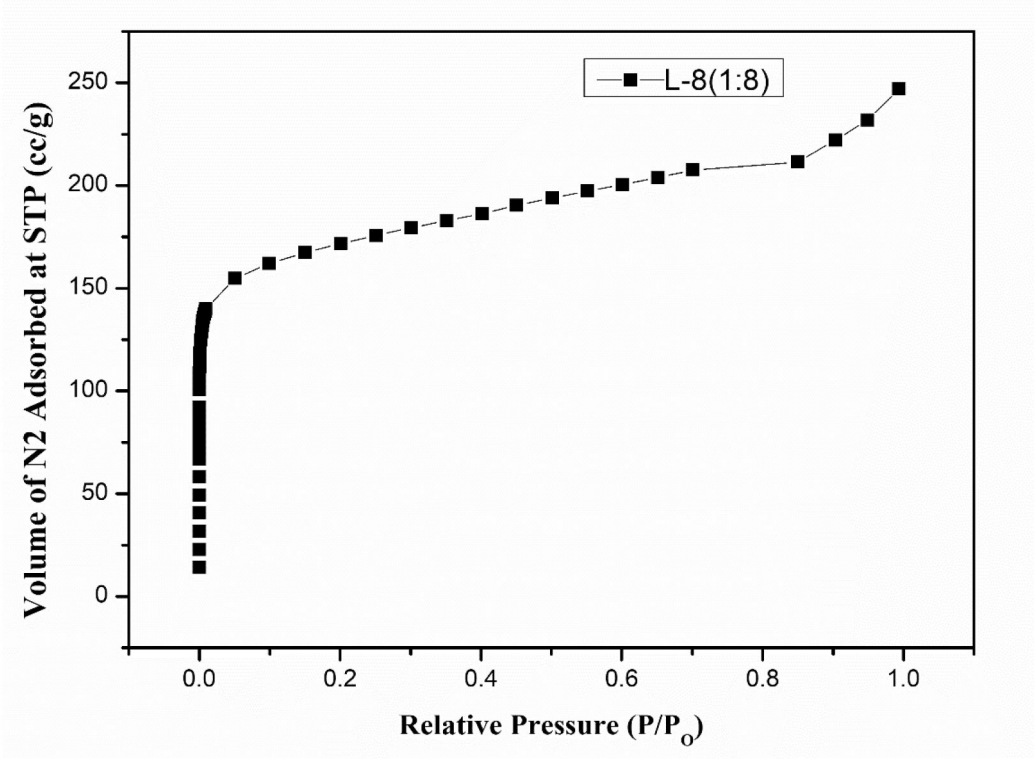

Figure 4. Volume of nitrogen adsorbed for L-8(1:8).

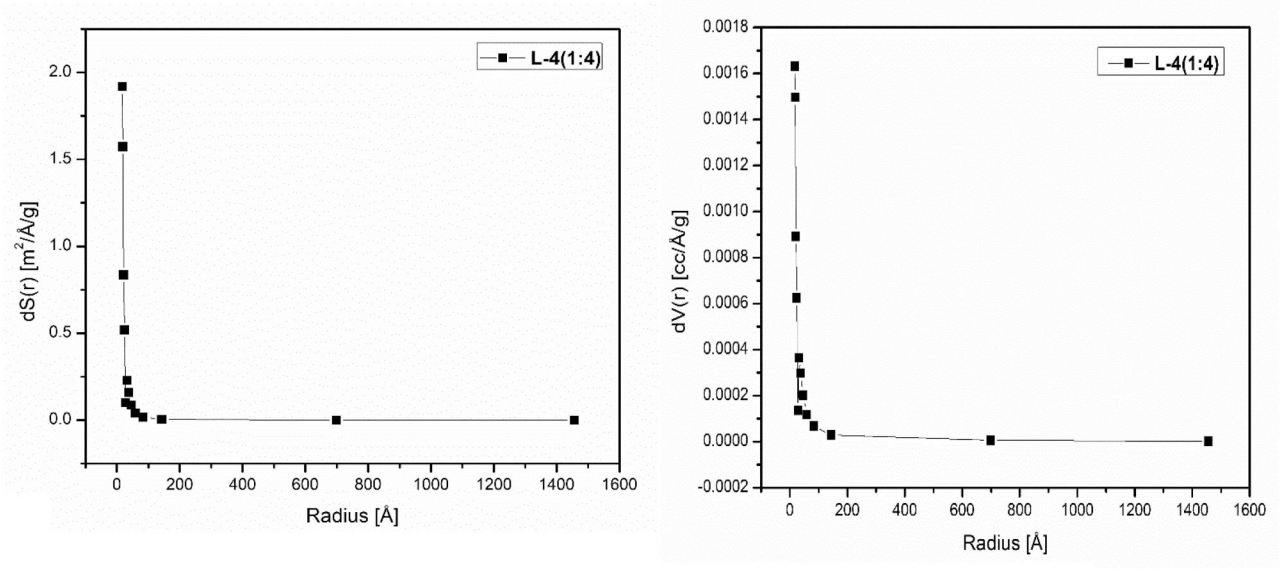

Figure 5. BJH pore size distribution of L-4(1:4).

difference distinguishes L-8(1:8) structurally from the other two samples. Medium, sharp O–H stretching bands between 3670–3681 cm^{-1} are present in L-4(1:4) and L-6(1:6), confirming alcohol groups. Notably, these peaks are absent in L-8(1:8), suggesting the lack of hydroxyl functionalities. This absence is beneficial because it minimizes competition between CO_2 and H_2O molecules for active sites, thereby improving adsorption efficiency under humid conditions. L-8(1:8) also exhibits C = O stretching vibrations, which are known to enhance both physisorption and chemisorption processes, further improving CO_2 uptake. The synergistic effect of these structural features optimizes CO_2–surface interactions, leading to higher adsorption capacity and selectivity. Thus, FTIR analysis confirms that L-8(1:8) possesses the most favorable surface chemistry for CO_2 adsorption among the studied samples, consistent with its enhanced performance in adsorption studies.[37]

Scanning electron microscopy

The surface morphology of AC samples prepared at different activation temperatures and impregnation ratios is presented in Figures 14–16.

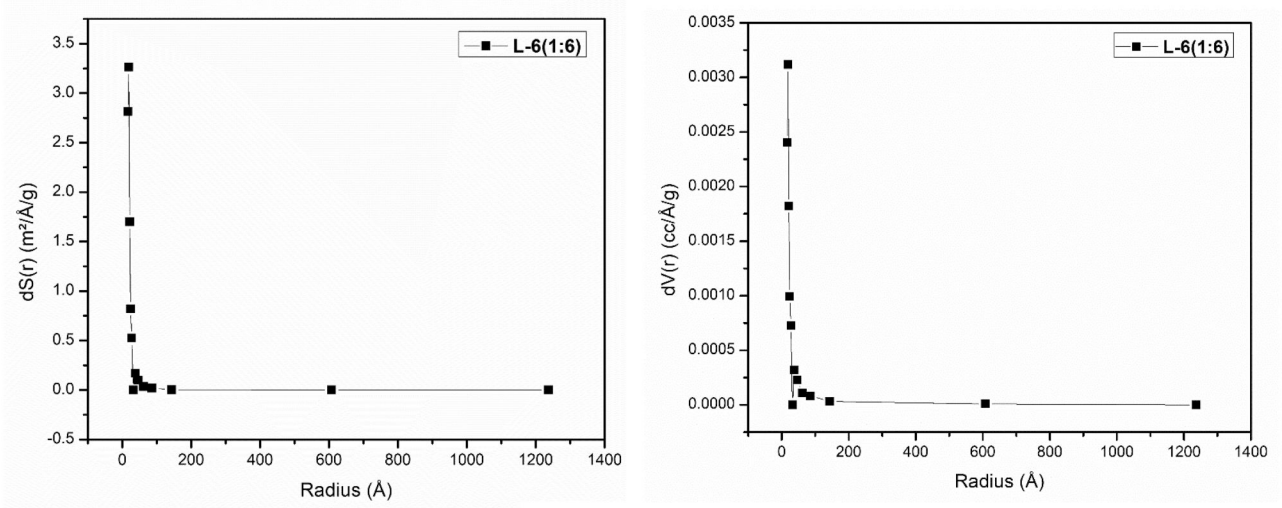

Figure 6. BJH pore size distribution of L-6 (1:6).

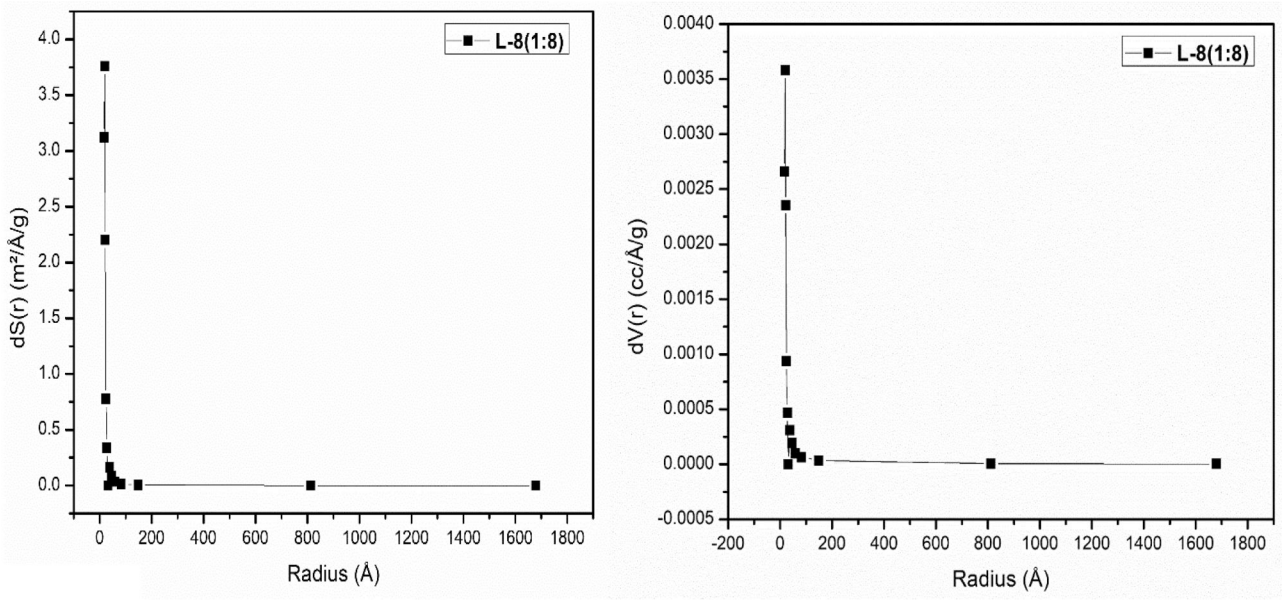

Figure 7. BJH pore size distribution of L-8(1:8).

During carbonization and subsequent activation, volatile components are released, leaving behind a fixed carbon framework. This process enhances the porosity of the material through the development and widening of pore networks. When KOH is used as the activating agent, it reacts with the carbon matrix *via* redox reactions, producing a well-developed porous carbon skeleton. These reactions not only generate new pores but also enlarge and stretch existing ones, thereby increasing the overall pore volume and surface area of the AC.[33] The scanning electron microscopy (SEM) micrographs reveal distinct surface features and variations in pore structures across the different samples. The presence of micropores is particularly significant, as they provide the active sites primarily responsible for gas adsorption. Thus, the pore development observed in the SEM images confirms the potential of the synthesized AC for effective adsorption applications.

XRD

XRD is a powerful analytical technique used to determine the atomic arrangement and crystalline properties of materials. When a crystalline sample is irradiated with X-rays, the atoms in its lattice scatter the incident radiation in specific directions. Constructive interference of these scattered beams produces a diffraction pattern, which can be analyzed to determine the structural order, crystallinity, and phase composition of the material. The XRD spectra of L-4(1:4), L-6(1:6), and L-8(1:8) samples are shown in Figures 17–19.

Prominent diffraction peaks were observed at $2\theta = 27.05°$ for L-4(1:4), $2\theta = 26.9°$ for L-6(1:6), and $2\theta = 26.9°$ for L-8(1:8), confirming the presence of crystallite structures in lignite-based AC. Highest peak intensity (198.85), indicating a relatively well-defined crystalline structure in L-4(1:4). Moderate peak intensity (163.02), suggesting partial crystallinity in L-6(1:6). Lowest peak intensity (114.14) in L-8(1:8)

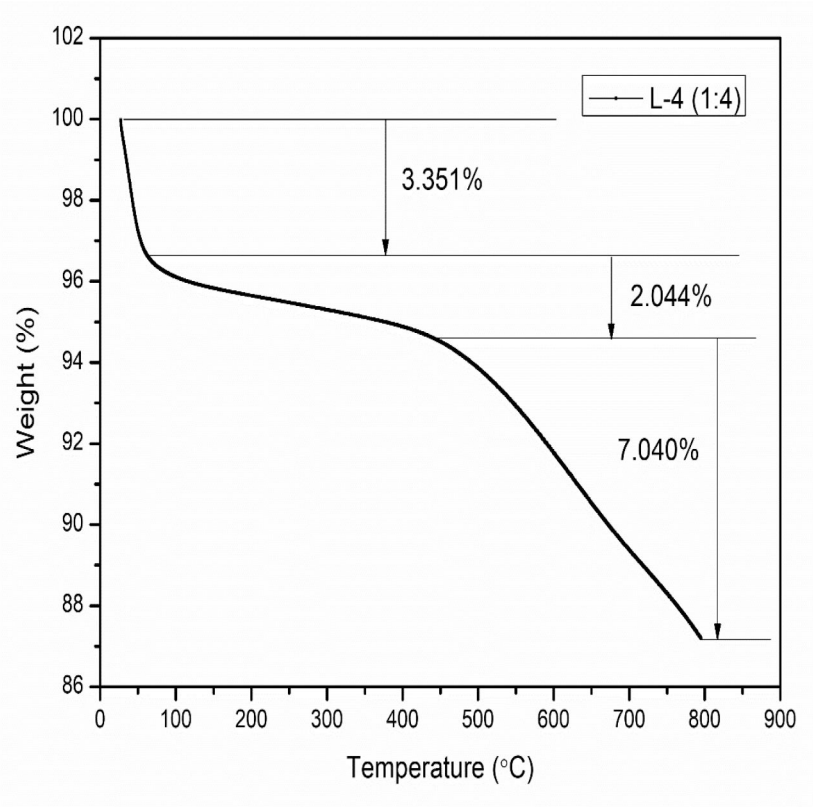

Figure 8. TGA for L-4(1:4) (weight vs temperature).

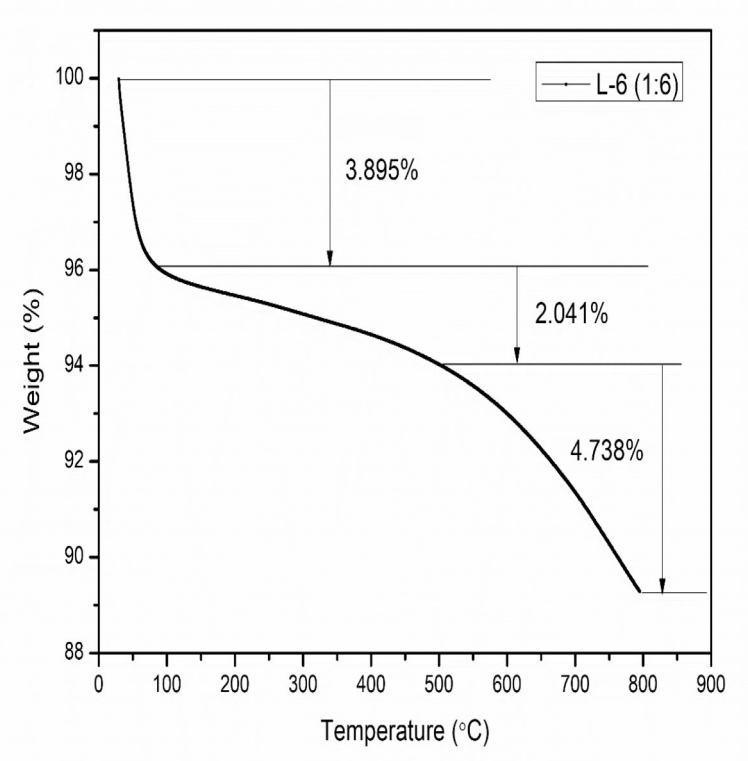

Figure 9. TGA for L-6(1:6) (weight vs temperature).

signifying a predominantly amorphous structure with reduced long-range order. Furthermore, L-4(1:4) and L-6(1:6) exhibited multiple diffraction peaks, while L-8(1:8) displayed fewer peaks, reinforcing its largely amorphous nature. From an adsorption perspective, the amorphous character of AC is highly desirable, as it enhances specific

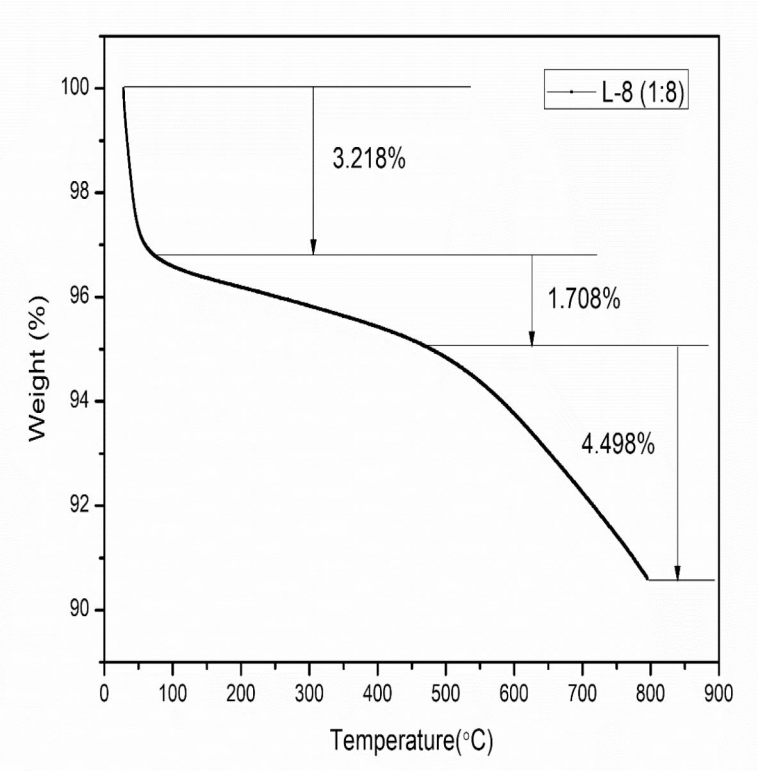

Figure 10. TGA for L-8(1:8) (weight vs temperature).

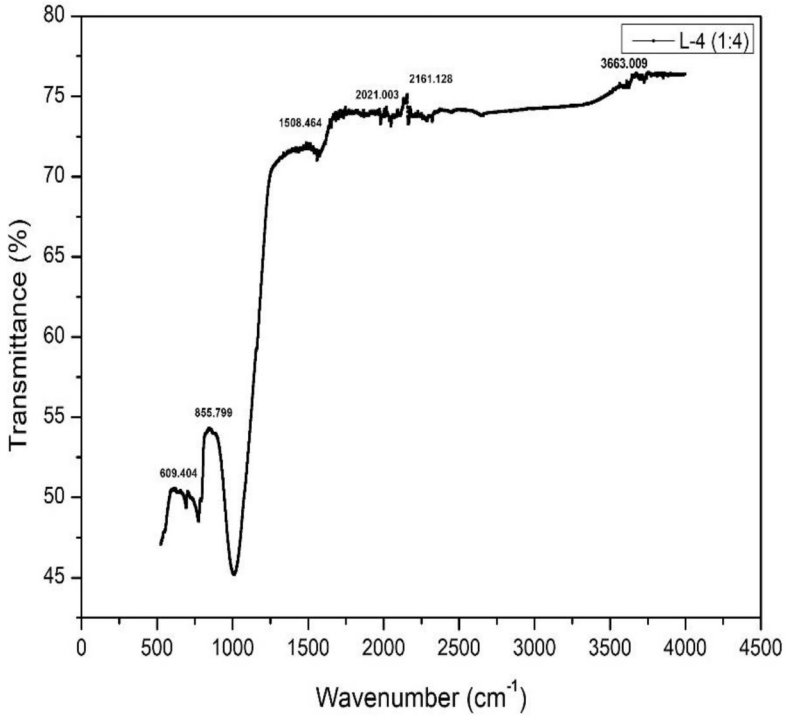

Figure 11. FTIR spectra of L-4(1:4).

surface area, pore volume, and the availability of active sites. Thus, the reduced crystallinity and more disordered structure of L-8(1:8) contribute to its superior adsorption capacity compared to L-4(1:4) and L-6(1:6).[38–39]

CO_2 adsorption experiment

Figures 20–22 present the CO_2 adsorption capacity as a function of relative pressure for the KOH-impregnated lignite coal samples. Batch adsorption experiments were

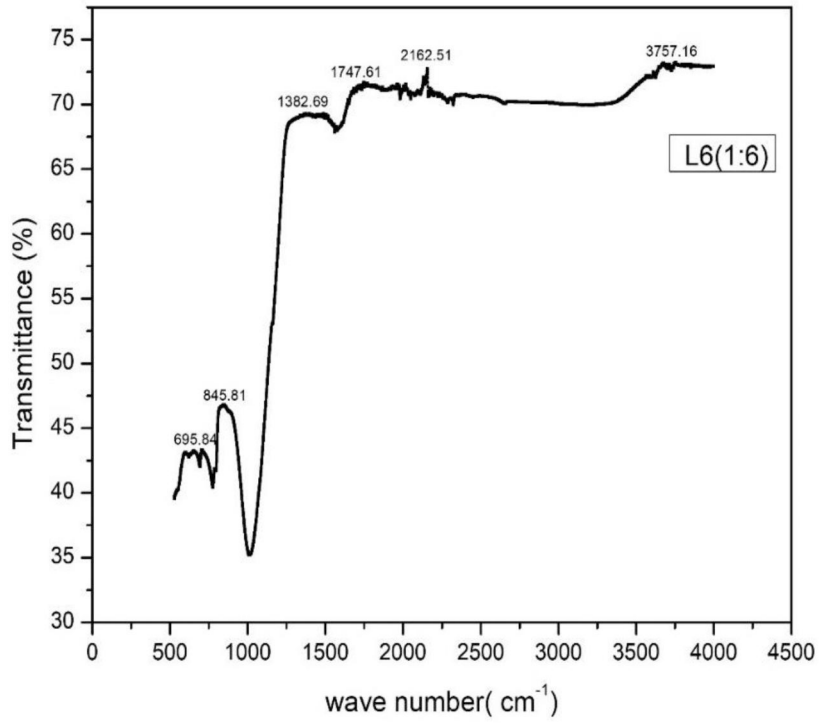

Figure 12. FTIR spectra of L-6(1:6).

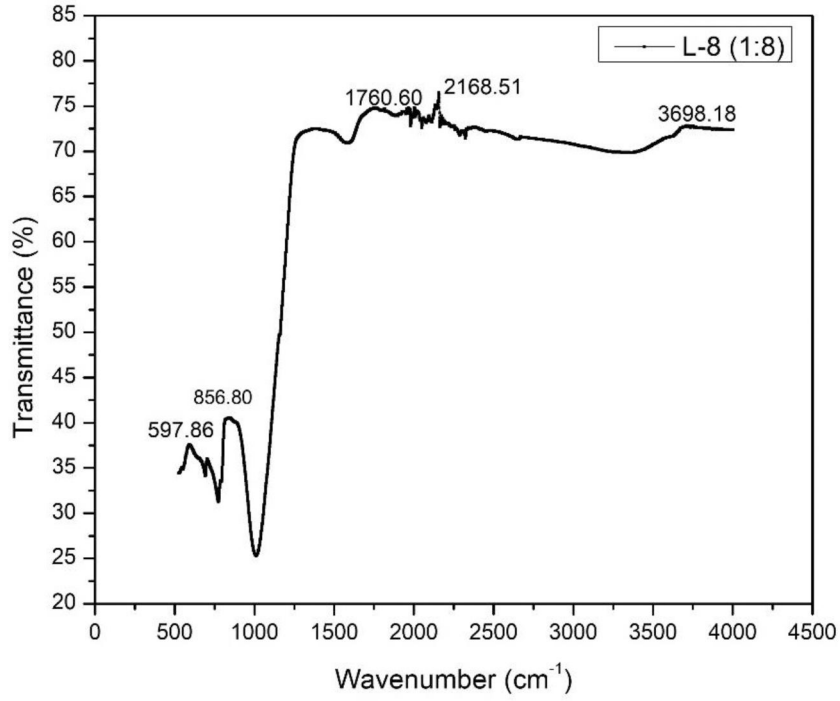

Figure 13. FTIR spectra of L-8(1:8).

conducted using an Autosorb iQ analyzer (Quanta Chrome Instruments) by the static volumetric method.

Prior to adsorption experiments, approximately 1 g of the AC sample was accurately weighed and loaded into a glass sample cell. Before analysis, samples were outgassed at 523 K for 6 h under high vacuum ($<10^{-5}$ mbar) to remove moisture and pre-adsorbed gases. until the system pressure reached atmospheric pressure. After degassing, the sample cell was isolated and cooled to the desired adsorption temperature. High-purity CO_2 (99.99%) was introduced stepwise up to 1 bar corresponding to a relative pressure (P/P_0) of unity, at 298 K under dry conditions.[28–29] Equilibrium adsorption was determined by pressure stabilization. Three consecutive adsorption–desorption cycles were carried out, with complete evacuation between cycles, to evaluate reversibility and adsorption stability. the CO_2 uptake was

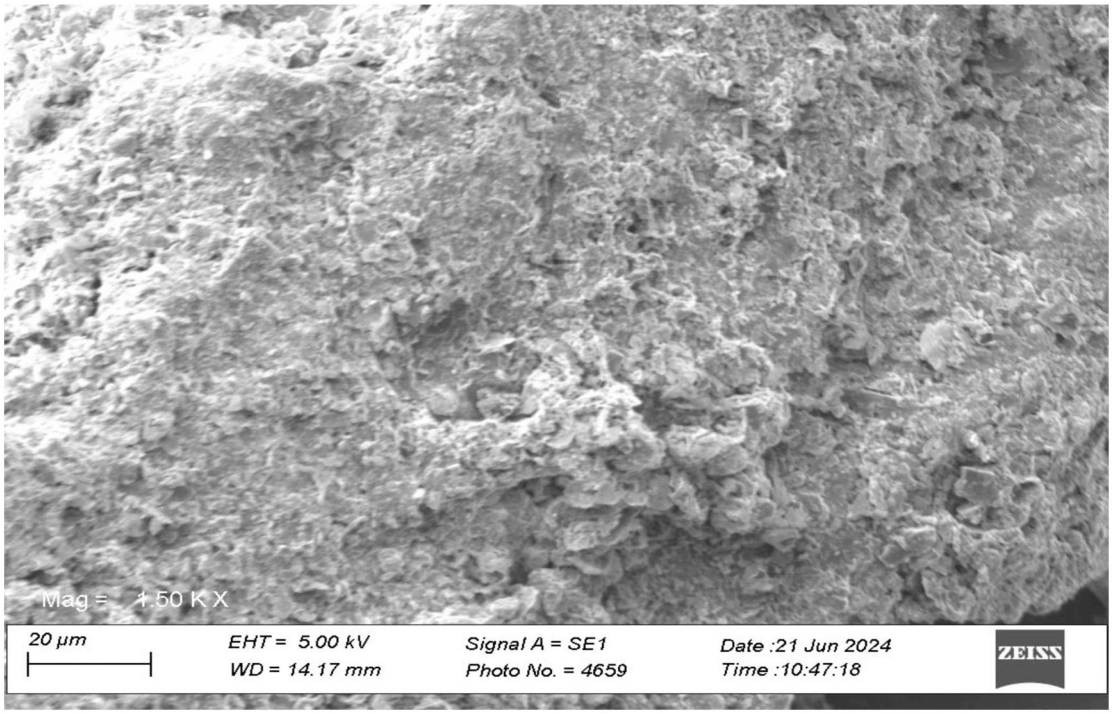

Figure 14. SEM image of L-4(1:4).

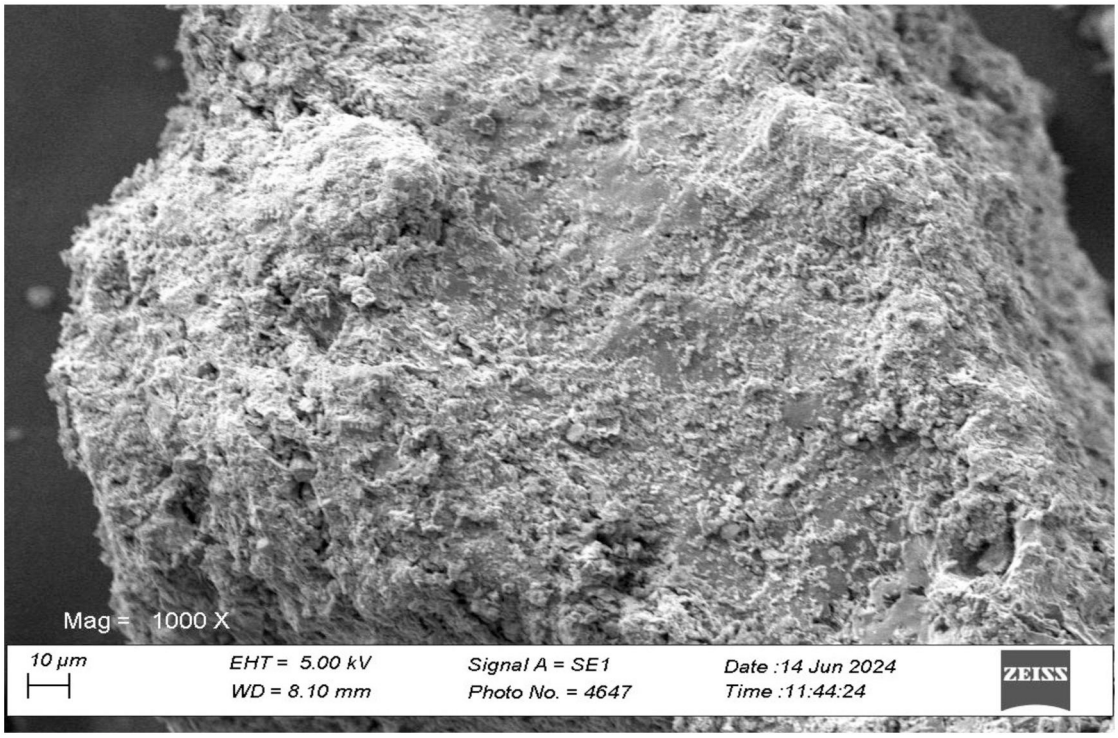

Figure 15. SEM image of L-6(1:6).

calculated automatically by the instrument software to generate adsorption isotherms. All adsorption experiments were conducted under well-controlled and stable conditions. The adsorption capacities of L-4(1:4), L-6(1:6), and L-8(1:8) were determined to be 13.8, 18.1, and 46.27 mg g^{-1}, respectively. Among these, the L-8(1:8) sample exhibited the highest CO_2 uptake, followed by L-6(1:6) and L-4(1:4). The enhanced adsorption performance of L-8(1:8) can be attributed to the chemical activation facilitated by KOH impregnation, which not only restricts tar formation but also promotes the development of an open porous structure. CO_2 uptake is attributed primarily to physisorption dominated by pore-filling in ultramicropores. Furthermore, increasing both the activation temperature and the impregnation ratio significantly improved the surface area of the lignite coal samples. This enhancement is primarily due to the removal of

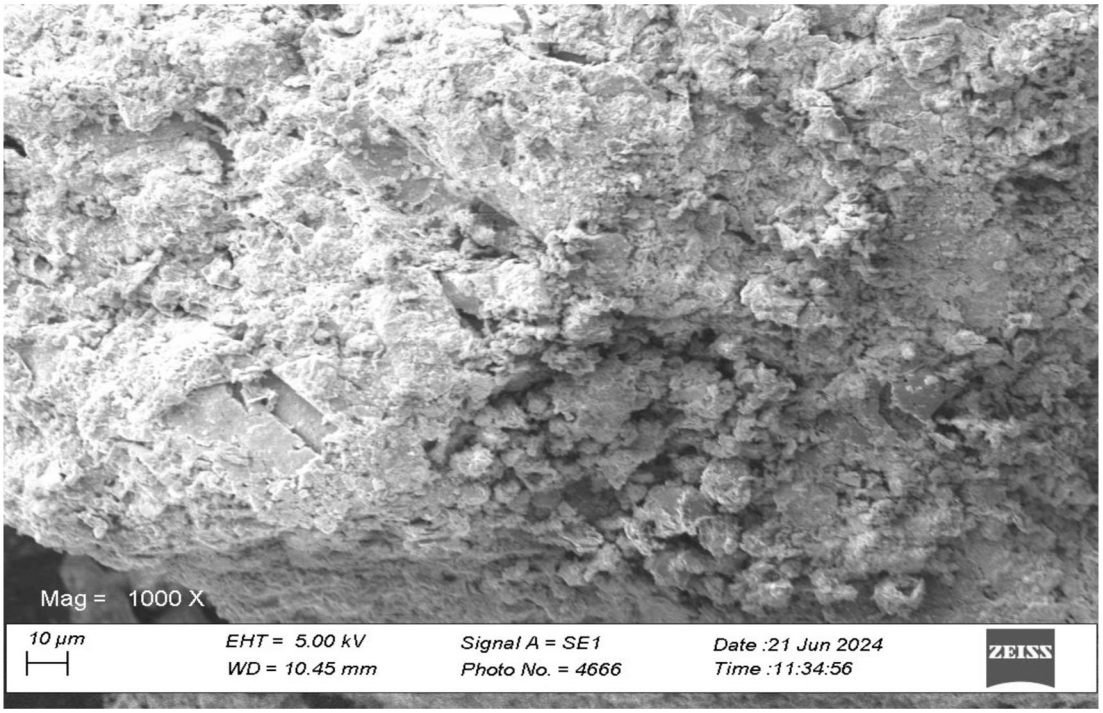

Figure 16. SEM image of L-8(1:8).

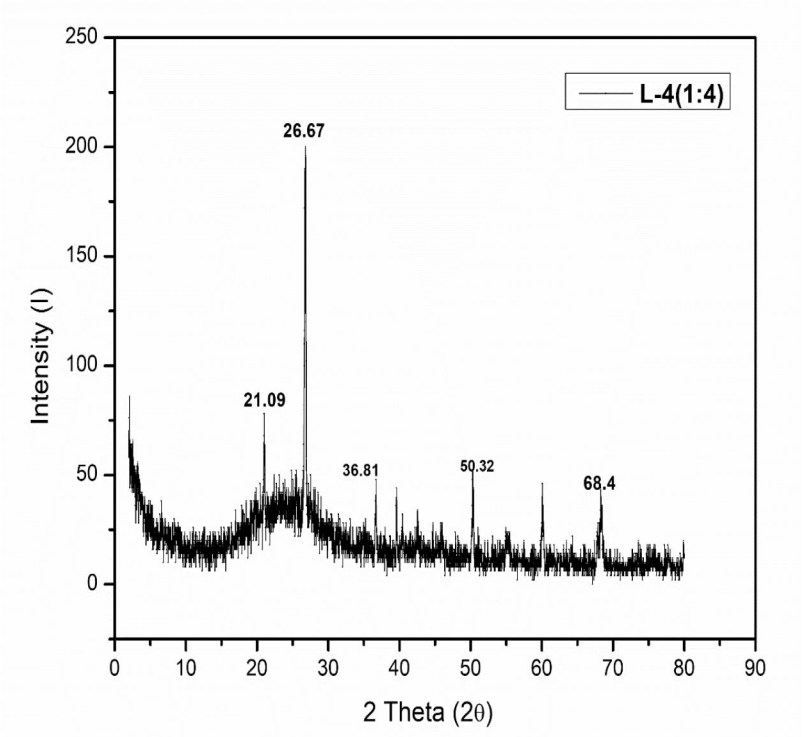

Figure 17. XRD spectra of L-4(1:4).

non-carbonaceous content and the interactions between KOH and the coal matrix, which contribute to the formation of additional pores. Consequently, higher impregnation ratios are favorable for the development of larger micropore volumes, thereby enhancing the overall CO_2 adsorption capacity.[40]

The present research is limited to equilibrium CO_2 uptake evaluation under fixed conditions without detailed adsorption isotherm fitting or kinetic modeling, which will be addressed in future work.

Breakthrough curve for CO_2 adsorption

Figure 23 illustrates the breakthrough curves for CO_2 adsorption on lignite-based AC samples. The experiments

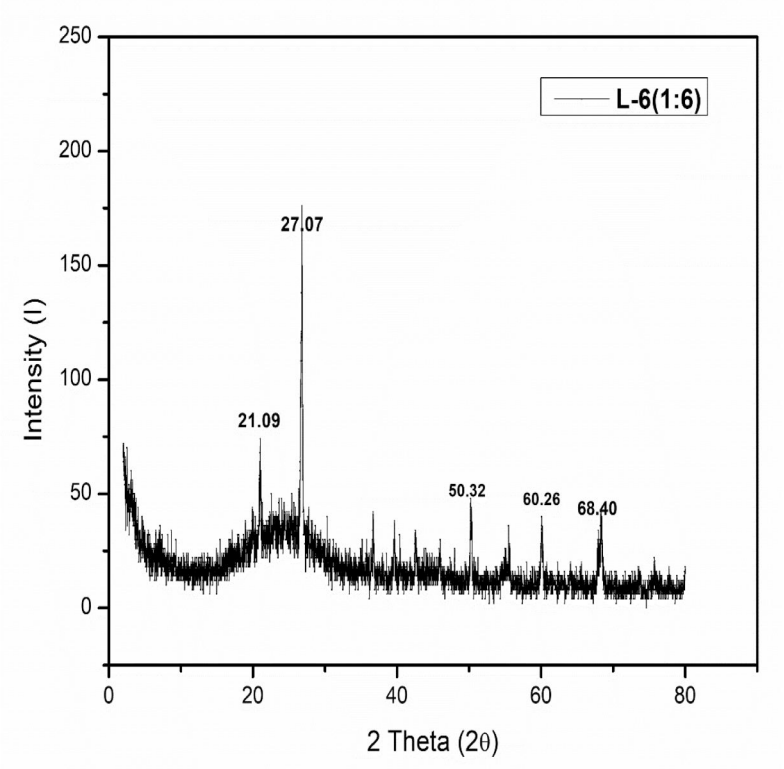

Figure 18. XRD spectra of L-6(1:6).

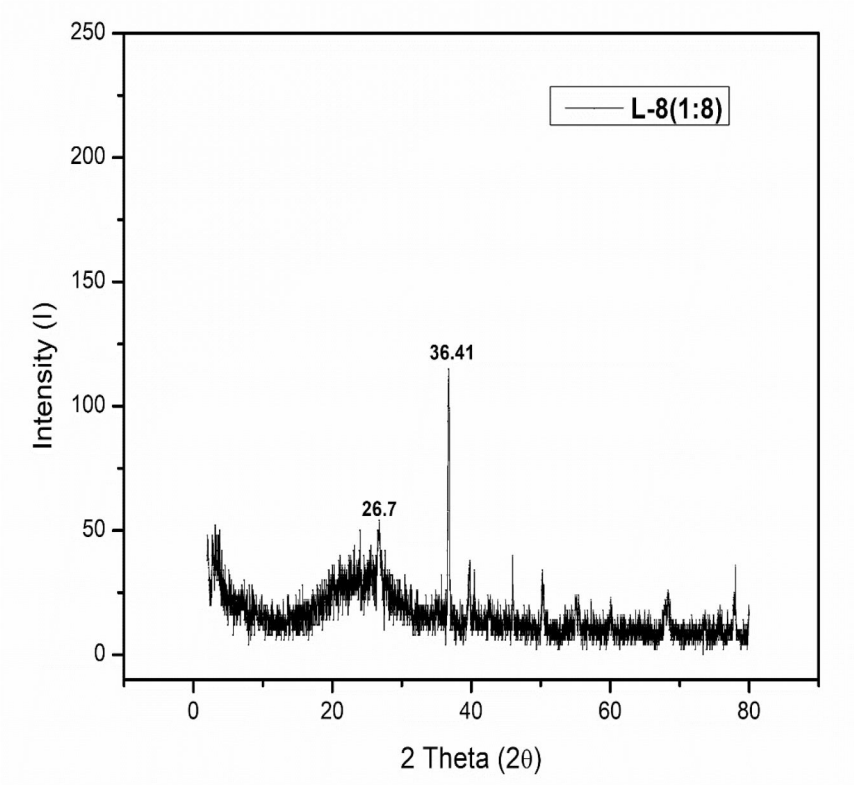

Figure 19. XRD spectra of L-8(1:8).

were conducted using an Automated Gas Sorption Analyzer (Autosorb iQ with ASiQwin software, Quantachrome Instruments). 1 g of the AC sample was packed into a glass sample tube of inner diameter 6 mm and length 100 mm serving as a micro-scale fixed-bed column. Prior to adsorption, all samples were outgassed at 523 K for 6 h until atmospheric pressure was attained followed by vacuum degassing ($<10^{-5}$ mbar) to ensure to remove moisture and pre-

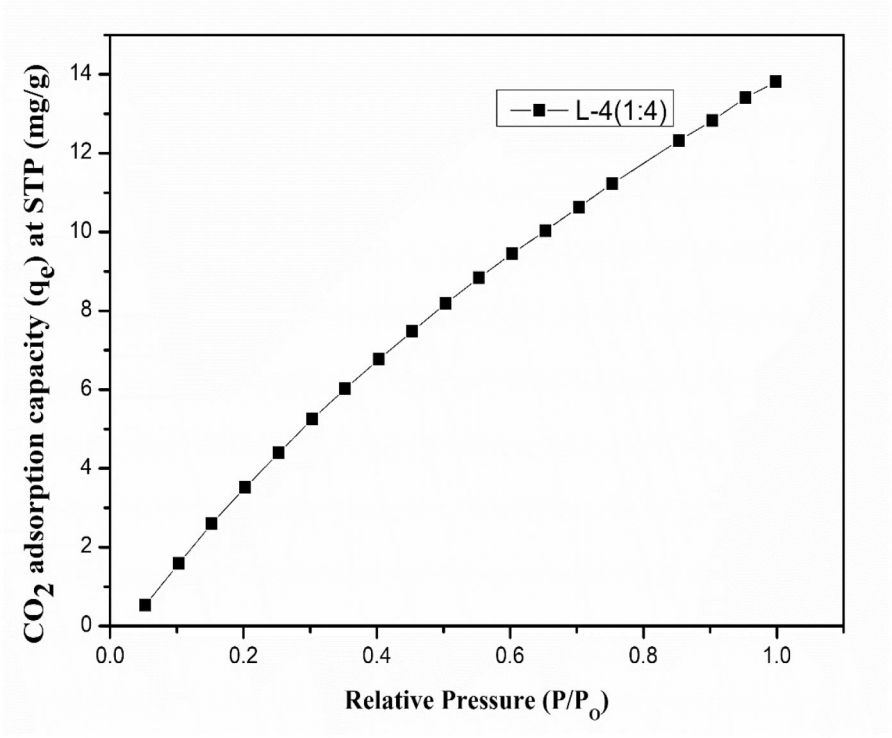

Figure 20. CO_2 adsorption capacity of L-4(1:4).

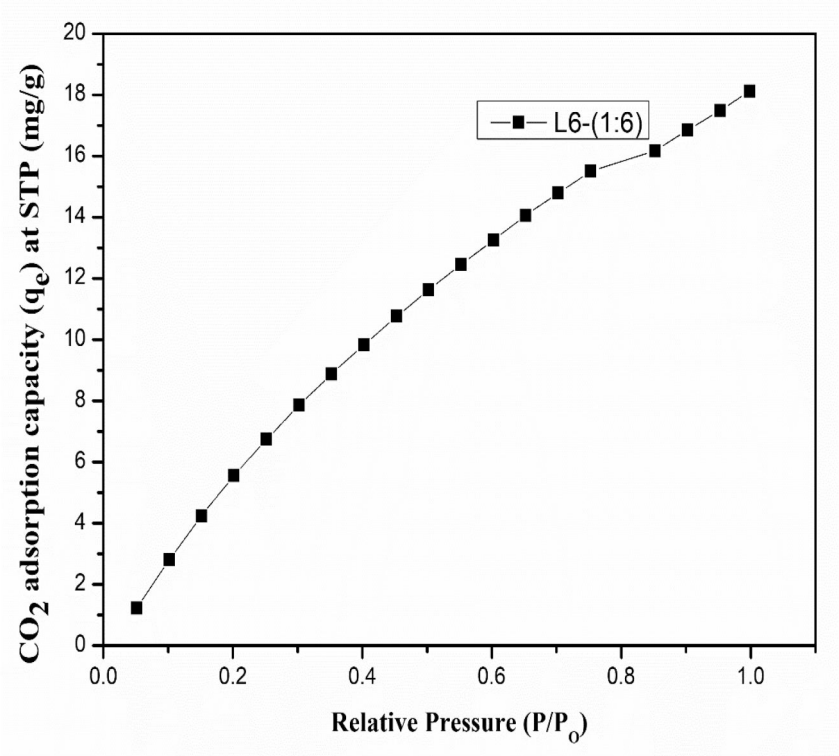

Figure 21. CO_2 adsorption capacity of L-6(1:6).

adsorbed gases and complete desorption of impurities. Inlet CO_2 (99.999% purity) was introduced at a controlled flow rate of 10 mL min^{-1}. The inlet CO_2 concentration was 1 bar pure CO_2. The CO_2 adsorption behavior was then evaluated at 298 K under varying time intervals at relative pressure ($P/P_0 = 1$).[29] The breakthrough profiles reveal that CO_2 uptake increases progressively with time until reaching a saturation point, beyond which adsorption capacity declines. The outlet gas composition was monitored continuously *via* the instrument's pressure-based detection system, allowing generation of adsorption vs. time (breakthrough) curves.

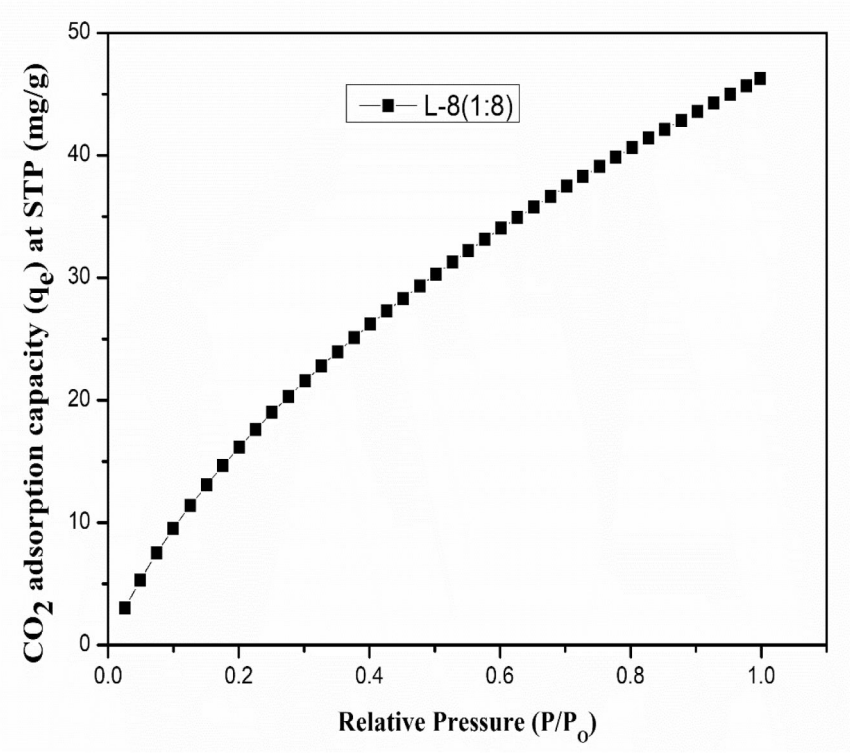

Figure 22. CO_2 adsorption capacity of L-8(1:8).

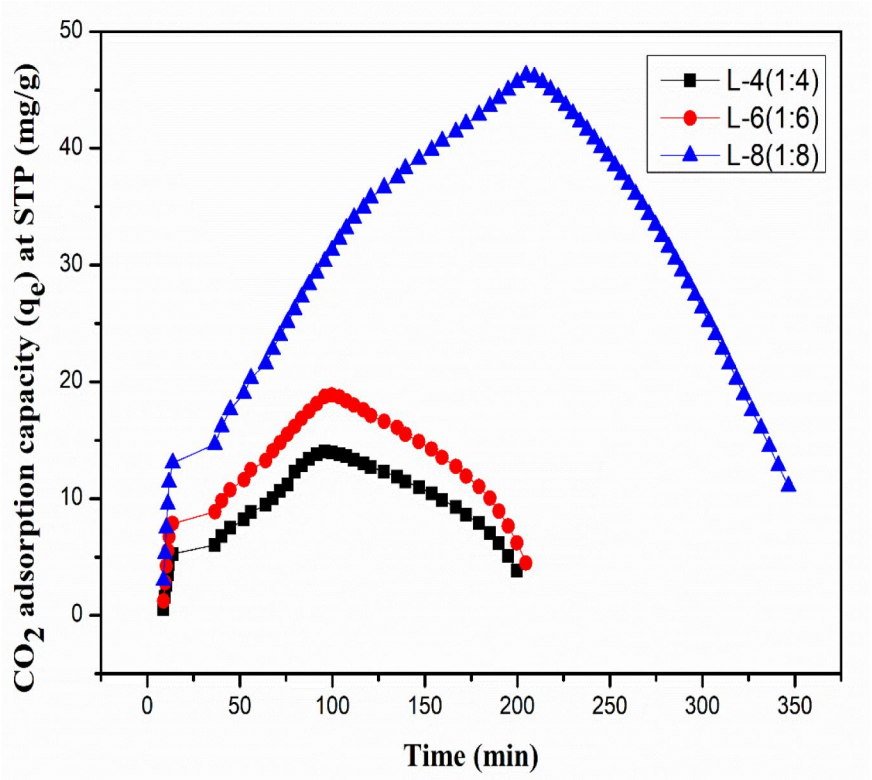

Figure 23. Breakthrough curve for CO_2 adsorption.

This trend was observed consistently across all investigated samples. The breakthrough time is directly related to adsorption capacity, with longer breakthrough times indicating superior CO_2 capture performance. The CO_2 adsorption capacities of L-4(1:4), L-6(1:6), and L-8(1:8) were measured to be 14.0, 18.8, and 46.27 mg g^{-1}, corresponding to breakthrough times of 95.9 min, 99.8 min, and 204.7 min, respectively. Among the tested sorbents, the L-8(1:8) sample exhibited the highest adsorption capacity and the longest breakthrough time, underscoring its superior performance.

Table 7. CO_2 adsorption capacity by different AC.

Sl no	Raw precursor	Activating agent	Temperature (°C)	Pressure (bar)	CO_2 uptake (mmol g^{-1})	Ref.
1	Potato starch and cellulose, eucalyptus sawdust	KOH	25	1	4.8	[41]
2	Borassus flabellifer flower (BFF)	KOH	25	1	4.82	[21]
3	Fern leaves	KOH	25	1	3.58	[42]
4	Hazelnut shell	KOH	25	1	4.23	[43]
5	Chest nut shell	KOH	25	1	3.61	[44]
6	Lemon peel waste	KOH	25	1	2.8	[45]
7	Garlic peel	KOH	25	1	4.22	[46]
8	Bituminous	KOH, NaOH, and $ZnCl_2$	25	1	9.09	[47]
9	Anthracite coal	KOH	25	1	10.51	[48]
10	Lignite coal	KOH,IR(1:8)	25	1	46.27 mg g^{-1}	This study

The study is limited to preliminary breakthrough evaluation and does not include moisture-containing gas performance. The adsorption performance of the KOH-activated lignite-derived AC was evaluated under controlled laboratory conditions using pure or simplified gas systems, and the cyclic adsorption–desorption stability was evaluated over a limited number of cycles.

Adsorption capacity for different materials activated with KOH for CO_2 capture

Table 7 represents a comparison of various carbon-based materials produced from different precursors and activated with KOH, focusing on their CO_2 uptake capacities under temperature 25 °C and pressure 1 bar. The CO_2 uptake was different for different due to the different impregnation ratio of KOH. The maximum CO_2 uptake for lignite coal with an impregnation ratio of 1:8 was 46.27 mg g^{-1} in this study.

Conclusions

In this study, coal-based AC was successfully synthesized and evaluated for CO_2 capture. Proximate analysis revealed that KOH impregnation significantly increased the fixed carbon content compared to the raw precursor, thereby enhancing adsorption potential. Lignite-based ACs demonstrated higher fixed carbon content than peat-based samples. Ultimate analysis further confirmed that the carbon content of KOH-impregnated ACs was greater than that of the raw and conventionally activated materials. Increasing the impregnation ratio led to a progressive enhancement in carbon content, favoring the development of efficient adsorbents. BET surface area analysis showed that lignite samples impregnated at ratios of 1:4, 1:6, and 1:8 exhibited the highest surface area, micropore area, and micropore volume, making them more suitable for adsorption than peat-derived ACs. Thermogravimetric analysis indicated total weight losses of 12.44%, 10.67%, and 9.42% for L-4(1:4), L-6(1:6), and L-8(1:8), respectively, with L-8(1:8) demonstrating superior thermal stability. FTIR spectra confirmed the presence of diverse functional groups in KOH-impregnated ACs. The significant pore development observed in the SEM images is for effective adsorption. Predominantly amorphous structure leads to superior adsorption capacity in L-8(1:8) adsorbent sample. Batch adsorption analysis established that CO_2 uptake was highest for L-8(1:8), i.e. 46.27 mg g^{-1}, due to the greater number of active sites and larger micropore area. The L-8(1:8) sample also exhibited the longest breakthrough time (204.7 min), further confirming its superior performance. Overall, among the investigated samples, lignite-derived AC with an impregnation ratio of 1:8 carbon exhibits superior CO_2 adsorption capacity and selectivity, due to its higher ultramicropore volume and favorable surface chemistry, and was identified as the most effective adsorbent for CO_2 capture, compared to samples with lower impregnation ratios. In addition to this, coal offers advantages in terms of consistent feedstock quality, large-scale availability, and ease of pore tuning, which are critical for industrial processes. Although the developed adsorbent showed high CO_2 adsorption capacity (46.27 mg g^{-1}) under controlled conditions, further validation under real flue gas environments, long-term cyclic operation, and techno-economic assessment is required to establish large-scale applicability.

Author contributions

CRediT: **Deepesh Kumar Biswal**: Data curation, Methodology, Writing – original draft; **Dipa Das**: Conceptualization, Formal analysis, Funding acquisition, Supervision; **Kashinath Barik**: Formal analysis, Visualization; **Sushanta Kumar Behera**: Conceptualization, Investigation, Validation, Visualization.

Disclosure statement

The authors declare no potential conflicts of interest.

Funding

This work was supported by the OURIIP Seed Funding sponsored by OSHEC and the Department of Chemical Engineering, Indira Gandhi Institute of Technology, Sarang, Odisha.

ORCID

Dipa Das http://orcid.org/0000-0002-7928-2404

Data availability statement

The datasets generated during the current study are available from the corresponding author on reasonable request.

References

[1] Lee, S. Y.; Park, S. J. A Review on Solid Adsorbents for Carbon Dioxide Capture. *J. Ind. Eng. Chem.* **2015**, *23*, 1–11. DOI: 10.1016/j.jiec.2014.09.001.

[2] Songolzadeh, M.; Soleimani, M.; Takht Ravanchi, M.; Songolzadeh, R. Carbon Dioxide Separation from Flue Gases: A Technological Review Emphasizing Reduction in Greenhouse Gas Emissions. *Sci. World J.* **2014**, *2014*, 828131–828134. DOI: 10.1155/2014/828131.

[3] Hussin, F.; Aroua, M. K. Recent Trends in the Development of Adsorption Technologies for Carbon Dioxide Capture: A Brief Literature and Patent Review (2014–2018). *J. Clean. Prod.* **2020**, *253*, 119707. DOI: 10.1016/j.jclepro.2019.119707.

[4] Raveendranathan, D. *Developments Lead to Pollution and Depletion of Natural Resources;* Notion Press Media Private Limited; Chennai, **2018**.

[5] Murty, J. V. S. Watershed Management, New Age International (P) Ltd. **1998**.

[6] Thiruvenkatachari, R.; Su, S.; An, H.; Yu, X. X. Post Combustion CO_2 Capture by Carbon Fibre Monolithic Adsorbents. *Prog. Energy Combust. Sci.* **2009**, *35*, 438–455. DOI: 10.1016/j.pecs.2009.05.003.

[7] Dantas, T. L.; Luna, F. M. T.; Silva, I. J.; Torres, A. E. B.; de Azevedo, D. C.; Rodrigues, A. E.; Moreira, R. F. Carbon Dioxide–Nitrogen Separation through Pressure Swing Adsorption. *Chem. Eng. J.* **2011**, *172*, 698–704. DOI: 10.1016/j.cej.2011.06.037.

[8] Choi, S.; Drese, J. H.; Jones, C. W. Adsorbent Materials for Carbon Dioxide Capture from Large Anthropogenic Point Sources. *ChemSusChem* **2009**, *2*, 796–854. DOI: 10.1002/cssc.200900036.

[9] Dechamps, P. CO_2 Capture and Storage Projects. *Eur. Comm. Rep.* **2007**, EUR 22574.

[10] Maroto-Valer, M. M.; Tang, Z.; Zhang, Y. CO_2 Capture by Activated and Impregnated Anthracites. *Fuel Process. Technol.* **2005**, *86*, 1487–1502. DOI: 10.1016/j.fuproc.2005.01.003.

[11] Pashaei, H.; Ghaemi, A. Review of CO_2 Capture Using Absorption and Adsorption Technologies. *Iran. J. Chem. Chem. Eng.* **2022**, *41*, 2771–2789.

[12] Stauffer, P. H.; Keating, G. N.; Middleton, R. S.; Viswanathan, H. S.; Berchtold, K. A.; Singh, R. P.; Mancino, A. Greening Coal: Breakthroughs and Challenges in Carbon Capture and Storage. *Energy Proc.* **2011**, *4*, 2955–2962.

[13] Quadrelli, R.; Peterson, S. The Energy–Climate Challenge: Recent Trends in CO_2 Emissions from Fuel Combustion. *Energy Policy* **2007**, *35*, 5938–5952. DOI: 10.1016/j.enpol.2007.07.001.

[14] Zangeneh, F. T.; Sahebdelfar, S.; Ravanchi, M. T. Conversion of Carbon Dioxide to Valuable Petrochemicals: An Approach to Clean Development Mechanism. *J. Nat. Gas Chem.* **2011**, *20*, 219–231. DOI: 10.1016/s1003-9953(10)60191-0.

[15] Plaza, M. G.; García, S.; Rubiera, F.; Pis, J. J.; Pevida, C. Post-Combustion CO_2 Capture with a Commercial Activated Carbon: Comparison of Different Regeneration Strategies. *Chem. Eng. J.* **2010**, *163*, 41–47. DOI: 10.1016/j.cej.2010.07.030.

[16] Ochedi, F. O.; Liu, Y.; Adewuyi, Y. G. State-of-the-Art Review on Capture of CO_2 Using Adsorbents Prepared from Waste Materials. *Process Saf. Environ. Prot.* **2020**, *139*, 1–25. DOI: 10.1016/j.psep.2020.03.036.

[17] Gunasekaran, P.; Veawab, A.; Aroonwilas, A. Corrosivity of Amine-Based Absorbents for CO_2 Capture. *Energy Proc.* **2017**, *114*, 2047–2054. DOI: 10.1016/j.egypro.2017.03.1339.

[18] Khraisheh, M.; Mukherjee, S.; Kumar, A.; Al Momani, F.; Walker, G.; Zaworotko, M. J. An Overview on Trace CO_2 Removal by Advanced Physisorbent Materials. *J. Environ. Manage.* **2020**, *255*, 109874. DOI: 10.1016/j.jenvman.2019.109874.

[19] Wong, S.; Bioletti, R. *Carbon Dioxide Separation Technologies*; Alberta Research Council: Edmonton, **2002**.

[20] Wilberforce, T.; Baroutaji, A.; Soudan, B.; Al-Alami, A. H.; Olabi, A. G. Outlook of Carbon Capture Technology and Challenges. *Sci. Total Environ.* **2019**, *657*, 56–72. DOI: 10.1016/j.scitotenv.2018.11.424.

[21] Tonu, N. T.; Kundu, S.; Islam, M. M.; Dhar, P. K.; Khandaker, T.; Anik, M. A. A. M.; Dutta, S. K.; Hasan, M. K.; Hossain, M. S. Fabrication of Waste Biomass-Derived KOH Activated Carbon for Enhanced CO_2 Capture. *New J. Chem.* **2024**, *48*, 20212–20224. DOI: 10.1039/D4NJ04495A.

[22] Deng, L.; Feng, D.; Zhang, W.; Yu, Y.; Sun, S.; Zhao, Y. Research on Biochar Prepared by Trace Koh Catalyzed CO_2 Activation vs Koh Activation as Advanced Candidate for Carbon Capture. SSRN 4985397. 2024, DOI: 10.2139/ssrn.4985397.

[23] Kundu, S.; Khandaker, T.; Anik, M. A.-A. M.; Hasan, M. K.; Dhar, P. K.; Dutta, S. K.; Latif, M. A.; Hossain, M. S. A Comprehensive Review of Enhanced CO2 Capture Using Activated Carbon Derived from Biomass Feedstock. *RSC Adv.* **2024**, *14*, 29693–29736. DOI: 10.1039/d4ra04537h.

[24] Khandaker, T.; Islam, T.; Nandi, A.; Anik, M. A. A. M.; Hossain, M. S.; Hasan, M. K.; Hossain, M. S. Biomass-Derived Carbon Materials for Sustainable Energy Applications: A Comprehensive Review. *Sustain. Energy Fuels* **2025**, *9*, 693–723. DOI: 10.1039/d4se01393j.

[25] Wang, X.; Zeng, W.; Kong, X.; Xin, C.; Dong, Y.; Hu, X.; Guo, Q. Development of Low-Cost Porous Carbons through Alkali Activation of Crop Waste for CO_2 Capture. *ACS Omega* **2022**, *7*, 46992–47001. DOI: 10.1021/acsomega.2c06109.

[26] Labus, K.; Gryglewicz, S.; Machnikowski, J. Granular KOH-Activated Carbons from Coal-Based Cokes and Their CO_2 Adsorption Capacity. *Fuel* **2014**, *118*, 9–15. DOI: 10.1016/j.fuel.2013.10.042.

[27] Das, D.; Samal, D. P.; Meikap, B. C. Preparation of Activated Carbon from Green Coconut Shell and Its Characterization. *J. Chem. Eng. Process Technol.* **2015**, *06*, 1000248. DOI: 10.4172/2157-7048.1000248.

[28] Das, D.; Meikap, B. C. Role of Amine-Impregnated Activated Carbon in Carbon Dioxide Capture. *Indian Chem. Eng.* **2021**, *63*, 435–447. DOI: 10.1080/00194506.2020.1760150.

[29] Das, D. Comparison of Adsorption Capacity of Amine-Modified Activated Carbon from Stone Apple for CO_2 Capture. *J. Inst. Eng. (India): Ser. E* **2024**, *104*, 1–15.

[30] Das, D.; Rautaray, S.; Barik, K.; Biswal, D. K. Comparative Analysis of CO_2 Adsorption Capacity for Amine-Modified Activated Carbon Prepared from Jujube Seed. In *International Conference on Pollution Control for Clean Environment*; Springer Nature: Singapore, **2023**; pp 107–116.

[31] Das, D.; Swain, L. Preparation and Characterization of Amine Modified Activated Carbon from Corncobs for Carbon Dioxide Capture. In *International Conference on Chemical, Bio and Environmental Engineering*; Springer: Cham, **2021**; pp 219–228.

[32] Şirazi, M.; Aslan, S. Comprehensive Characterization of High Surface Area Activated Carbon Prepared from Olive Pomace by KOH Activation. *Chem. Eng. Commun.* **2021**, *208*, 1479–1493. DOI: 10.1080/00986445.2020.1864628.

[33] Mistar, E. M.; Alfatah, T.; Supardan, M. D. Synthesis and Characterization of Activated Carbon from Bambusa Vulgaris Striata Using Two-Step KOH Activation. *J. Mater. Res. Technol.* **2020**, *9*, 6278–6286. DOI: 10.1016/j.jmrt.2020.03.041.

[34] Yorgun, S.; Yıldız, D. Preparation and Characterization of Activated Carbons from Paulownia Wood by Chemical Activation with H_3PO_4. *J. Taiwan Inst. Chem. Eng.* **2015**, *53*, 122–131. DOI: 10.1016/j.jtice.2015.02.032.

[35] Raymundo-Piñero, E.; Azaïs, P.; Cacciaguerra, T.; Cazorla-Amorós, D.; Linares-Solano, A.; Béguin, F. KOH and NaOH Activation Mechanisms of Multiwalled Carbon Nanotubes with Different Structural Organisation. *Carbon N Y* **2005**, *43*, 786–795. DOI: 10.1016/j.carbon.2004.11.005.

[36] Thommes, M.; Kaneko, K.; Neimark, A. V.; Olivier, J. P.; Rodriguez-Reinoso, F.; Rouquerol, J.; Sing, K. S. W.

Physisorption of Gases, with Special Reference to the Evaluation of Surface Area and Pore Size Distribution (IUPAC Technical Report). *Pure Appl. Chem.* **2015**, *87*, 1051–1069. DOI: 10.1515/pac-2014-1117.

[37] Wazir, A. H.; Haq, I. U.; Manan, A.; Khan, A. Preparation and Characterization of Activated Carbon from Coal by Chemical Activation with KOH. *Int. J. Coal Prep. Util.* **2022**, *42*, 1477–1488. DOI: 10.1080/19392699.2020.1727896.

[38] Li, L.; Sun, F.; Gao, J.; Wang, L.; Pi, X.; Zhao, G. Broadening the Pore Size of Coal-Based Activated Carbon via a Washing-Free Chem-Physical Activation Method for High-Capacity Dye Adsorption. *RSC Adv.* **2018**, *8*, 14488–14499. DOI: 10.1039/c8ra02127a.

[39] Li, D.; Zhou, J.; Wang, Y.; Tian, Y.; Wei, L.; Zhang, Z.; Qiao, Y.; Li, J. Effects of Activation Temperature on Densities and Volumetric CO_2 Adsorption Performance of Alkali-Activated Carbons. *Fuel* **2019**, *238*, 232–239. DOI: 10.1016/j.fuel.2018.10.122.

[40] Ogungbenro, A. E.; Quang, D. V.; Al-Ali, K. A.; Vega, L. F.; Abu-Zahra, M. R. Synthesis and Characterization of Activated Carbon from Biomass Date Seeds for Carbon Dioxide Adsorption. *J. Environ. Chem. Eng.* **2020**, *8*, 104257. DOI: 10.1016/j.jece.2020.104257.

[41] Sevilla, M.; Fuertes, A. B. Sustainable Porous Carbons with a Superior Performance for CO_2 Capture. *Energy Environ. Sci.* **2011**, *4*, 1765–1771. DOI: 10.1039/c0ee00784f.

[42] Serafin, J.; Dziejarski, B.; Vendrell, X.; Kiełbasa, K.; Michalkiewicz, B. Biomass Waste Fern Leaves as a Material for a Sustainable Method of Activated Carbon Production for CO_2 Capture. *BMSBEO* **2023**, *175*, 106880. DOI: 10.1016/j.biombioe.2023.106880.

[43] Pang, R.; Lu, T.; Shao, J.; Wang, L.; Wu, X.; Qian, X.; Hu, X. Highly Efficient Nitrogen-Doped Porous Carbonaceous CO_2 Adsorbents Derived from Biomass. *Energy Fuels* **2020**, *35*, 1620–1628. DOI: 10.1021/acs.energyfuels.0c03832.

[44] Li, Q.; Liu, S.; Peng, W.; Zhu, W.; Wang, L.; Chen, F.; Shao, J.; Hu, X. Preparation of Biomass-Derived Porous Carbons by a Facile Method and Application to CO_2 Adsorption. *J. Taiwan Inst. Chem. Eng.* **2020**, *116*, 128–136. DOI: 10.1016/j.jtice.2020.11.001.

[45] Weldekidan, H.; Patel, H.; Mohanty, A.; Misra, M. Synthesis of Porous and Activated Carbon from Lemon Peel Waste for CO_2 Adsorption. *Carbon Capture Sci. Technol.* **2024**, *10*, 100149. DOI: 10.1016/j.ccst.2023.100149.

[46] Huang, G.; Wu, X.; Hou, Y.; Cai, J. Sustainable Porous Carbons from Garlic Peel Biowaste and KOH Activation with an Excellent CO_2 Adsorption Performance. *Biomass Conv. Bioref.* **2020**, *10*, 267–276. DOI: 10.1007/s13399-019-00412-6.

[47] Toprak, A.; Kopac, T. Carbon Dioxide Adsorption Using High Surface Area Activated Carbons from Local Coals Modified by KOH, NaOH and $ZnCl_2$ Agents. *Int. J. Chem. React. Eng.* **2017**, *15*, 20160042. DOI: 10.1515/ijcre-2016-0042.

[48] Hamyali, H.; Nosratinia, F.; Rashidi, A.; Ardjmand, M. Anthracite Coal-Derived Activated Carbon as an Effectiveness Adsorbent for Superior Gas Adsorption and CO_2/N_2 and CO_2/CH_4 Selectivity: Experimental and DFT Study. ***J.*** *Environ. Chem. Eng.* **2022**, *10*, 107007. DOI: 10.1016/j.jece.2021.107007.